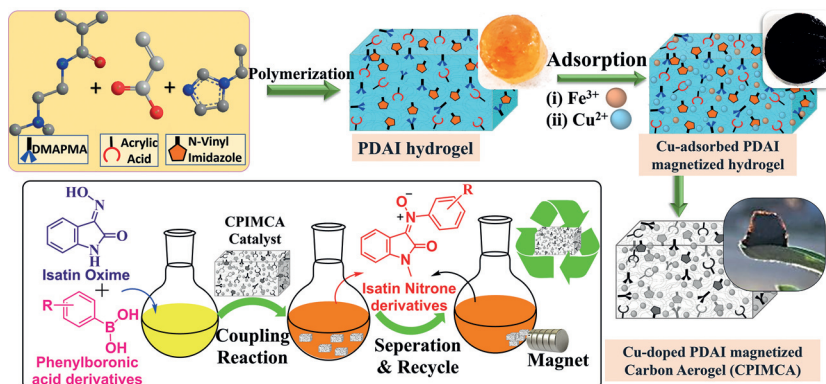


Exploring the Catalytic Efficiency of Copper-Doped Magnetic Carbon Aerogel for the Coupling Reaction of Isatin Oxime with Phenylboronic Acid Derivatives

Deeksha Mudgal
Ravi Pratap Singh
Nisha Yadav
Tapeesh Bharti
Vivek Mishra*

Amity Institute of Click Chemistry Research and Studies (AICCRS),
Amity University Noida, UP-201313, India
vmishra@amity.edu



Received: 28.07.2023

Accepted after revision: 21.09.2023

Published online: 27.09.2023 (Accepted Manuscript), 09.11.2023 (Version of Record)

DOI: 10.1055/a-2182-7757; Art ID: SO-2023-07-0053-OP

License terms:

© 2023. The Author(s). This is an open access article published by Thieme under the terms of the Creative Commons Attribution License, permitting unrestricted use, distribution and reproduction, so long as the original work is properly cited. (<https://creativecommons.org/licenses/by/4.0/>)

Abstract A highly efficient catalyst, Cu-doped poly(*N*-[3-(dimethylamino)propyl]methacrylamide, acrylic acid, *N*-vinyl imidazole) (PDAI) magnetic carbon aerogel (CPIMCA), was successfully employed for the synthesis of isatin nitrone derivatives. The 3D porous CPIMCA catalyst demonstrated outstanding performance through the application of a coupling reaction between isatin oxime and phenylboronic acid derivatives, providing up to 98% yield of the required nitrone derivatives. Remarkably, the incorporation of copper within the polymeric structure of the magnetic carbon aerogel exhibited a significant influence on catalytic activity, even at a low overall copper content of approximately 2%. This was confirmed through EDX elemental mapping analysis, further establishing the competence of the catalyst for catalytic reactions. Comparative studies revealed that CPIMCA outperformed Cu(OAc)₂ catalyst, providing a notable 10–15% increase in product yield. This superior performance can be attributed to the unique synergistic effect of copper, iron, and carbon aerogel as the polymeric matrix, highlighting the exceptional capabilities of CPIMCA as a catalyst.

Keywords catalytic coupling reaction, recyclable magnetic catalyst, carbon aerogel, iron, copper doping

Selective and efficient synthesis of heteroatomic compounds plays a crucial role in the preparation of various pharmaceuticals, agrochemicals, and functional materials. The synthesis of many different organic molecules depends on catalytic coupling processes, which have attracted a lot of interest in the field of organic chemistry.^{1–4} These processes, which result in the formation of new carbon–carbon

or carbon–heteroatom bonds, provide an adaptable and successful method for developing complex compounds. Among the different approaches, catalytic methods have gained considerable attention due to their environmentally friendly nature and mild reaction conditions. Coupling and cross-coupling reactions use metal-based catalysts such as palladium, platinum, and rhodium, and some reactions specifically use heavy metals like mercury, lead, or cadmium, which can pose environmental and health risks and are highly expensive and non-recoverable.^{5–14} In coupling reactions, the metal catalysts can be prone to poisoning or deactivation by various species present in the reaction mixture.¹⁴ The release of these metals or their derivatives into the environment during catalytic processes can be harmful to ecosystems and human health. Making the reaction cost-prohibitive and not favorable to the environment are other factors. The greatest disadvantage of using heavy catalysts is that they are not recoverable and can be used only a single time.^{15,16} Some nano techniques are used to deal with the disposed metals, such as nanoparticles, nanotubes, and carbon-based materials.^{17–19} To enhance the efficiency and selectivity of these reactions, studies have focused on acquiring advanced catalysts that exhibit remarkable catalytic properties and will also be more eco-friendly.^{4,20,21}

Carbon aerogels are highly porous materials with a three-dimensional network structure, providing a large surface area and excellent stability. In recent years, carbon-based catalysts have emerged as promising candidates for organic transformations owing to their unique properties and tunable reactivity. Vinyl-based hydrophilic co-monomers; *N*-[3-(dimethylamino)propyl]methacrylamide (DMAPMA), acrylic acid (Aac), and *N*-vinyl Imidazole (NVI) make a promising polymer (referred to as PDAI). The presence of

polar functional groups in vinyl-based monomers, such as amine or carboxyl groups, imparts hydrophilic properties to the resulting aerogel.²² Notably, DMAPMA can be polymerized readily in aqueous medium with other monomers; while acrylic monomers make polymers more flexible and control hardness, in *N*-vinyl imidazole, the imidazole moiety endows hydrophilicity to the resulting hydrogel. Furthermore, imidazole groups have the ability to create coordination bonds with metal ions, resulting in the formation of metal-polymer complexes.^{23–26}

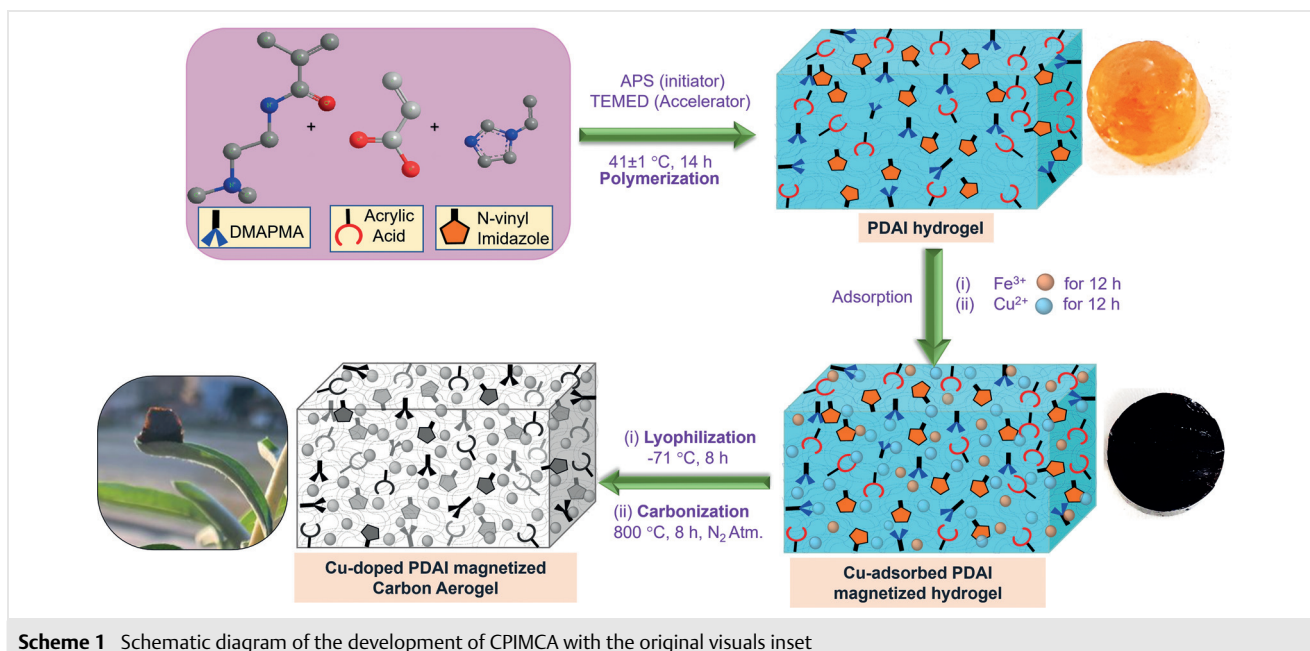
Moreover, allowing the incorporation of copper and iron into carbon aerogels adds the advantages of facile separation and recyclability, minimizing the environmental impact and improving the overall sustainability of the process. Interestingly, copper activates C–H bonds, and iron makes the carbon aerogel magnetic, enabling multiple cycles of catalytic reactions by facilitating its recovery after reaction completion. Copper itself is a proficient catalyst, so incorporation of copper is a greener strategy because it is economical and one of the most abundant elements on earth. Compared to expensive metal catalysts, copper catalysts often work under less adverse conditions. It is potentially selective towards C–N, C–C, and C–O bonds by varying the reaction conditions in different coupling reactions.^{27–31} A variety of schemes are already known for the synthesis of isatin nitrones using different reaction conditions. Chen et al. and Mo et al.^{32,33} synthesized the nitrone product using $\text{Cu}(\text{Oac})_2$ as catalyst in different solvents to select the best solvent to achieve the highest yield. To improve on these results, the primary goal of this research was to create a magnetic carbon aerogel catalyst with copper doping and to evaluate the catalytic performance for the selective *N*-arylation reaction of isatin oxime with phenylboronic acid derivatives. The integration of copper and iron into the carbon aerogel matrix provides a synergistic effect, combining the unique properties of carbon aerogels with the catalytic activity of copper. To achieve this goal, catalyst synthesis was carried out via the co-polymerization procedure, and the adsorption of Fe and Cu inside the polymeric structure was done via the in-situ adsorption method. This synthetic method produces a high-quality hydrophilic copper- and iron-adsorbed hydrogel, which was then lyophilized and further carbonized to produce the Cu-doped PDAI magnetic carbon aerogel (CPIMCA). In addition, morphological and chemical characterization of the synthesized catalyst was done with a range of analytical techniques, such as FTIR, vibration sample magnetometry (VSM), X-ray diffraction (XRD), scanning electron microscopy (SEM), energy-dispersive X-ray (EDX), transition electron microscopy (TEM), and X-ray photoelectron spectroscopy (XPS). Overall, this research presents an innovative approach to developing a highly efficient and recyclable catalyst for catalytic coupling reactions. The unique combination of copper and magnetic

carbon aerogels offers significant potential for the advancement of catalysis, enabling the synthesis of complex organic molecules with improved efficiency and selectivity.

Synthesis of Cu-Doped PDAI Magnetic Carbon Aerogel (CPIMCA)

PDAI hydrogel was created by the free radical copolymerization method, in which the monomers were polymerized through vinyl bonds, leading to the formation of a polymeric matrix. In the synthetic procedure for the generation of PDAI hydrogel, the monomers DMAPMA, Aac, and *N*-vinyl imidazole were first mixed sequentially in volumes of 1.44, 1.12, and 0.24 mL, respectively. All three vinyl monomers were dissolved in 1.56 mL of distilled water in an ice-bath. Shortly after thoroughly mixing the monomers with distilled water, 100 μL of APS was added as initiator, which initiated the cleavage of vinyl bonds in the monomers, making the free radicals available for chain initiation. After homogenizing the monomeric mixture to begin the polymerization process, 2.5 μL of accelerator TEMED was blended consistently to accelerate the reaction for chain propagation, maintaining the temperature at below 10 °C.^{25,34}

After homogenizing the mixture, it was transferred to a test tube and kept at 41 ± 1 °C (Scheme 1). After 14 h of heating in an oil bath, the PDAI hydrogel was produced. The formed hydrogel was washed with water three times to pull out the remaining unreacted monomers that might still be present. The material was then dried at 60 °C in an oven. Once dried, the hydrogel was magnetized by submerging it in a solution containing both $\text{FeSO}_4 \cdot 7\text{H}_2\text{O}$ and $\text{FeCl}_3 \cdot 6\text{H}_2\text{O}$ to adsorb Fe ions.³⁵ Following alkali treatment, the magnetized hydrogel was kept in an aqueous ammonia solution overnight to reduce Fe^{3+} and Fe^{2+} . After the adsorption of the Fe onto the surface of the hydrogel, the material was dipped in a solution of $\text{CuCl}_2 \cdot 2\text{H}_2\text{O}$ to adsorb copper. All three ions, $\text{FeSO}_4 \cdot 7\text{H}_2\text{O}$, $\text{FeCl}_3 \cdot 6\text{H}_2\text{O}$, and $\text{CuCl}_2 \cdot 2\text{H}_2\text{O}$, were taken in a ratio of 1:2:1. Once the Cu and Fe adsorption was complete, the PDAI hydrogel was freeze-dried or lyophilized at -71 °C for 8 h in order to evaporate the water.³⁶ This is the most important step in the process of aerogel formation; all the water from the polymeric matrix is removed while maintaining the internal structure of the aerogel. Subsequently, to form a carbon magnetic aerogel, the prepared aerogel was treated at 800 °C for 8 h in an inert atmosphere with a heating rate of 4 °C/min in a tube furnace for carbonization. During carbonization, the adsorbed ions of Cu and Fe were incorporated inside the carbon structure of the polymer. Hence, carbonization also facilitates the incorporation of Cu and Fe inside the polymeric chain; this, in turn, leads to the electrostatic binding of copper and iron to the carbon structure, which, consequently, makes it possible for copper to be doped onto PDAI carbon aerogel.



Catalytic Activity of As-Synthesized CPIMCA for *N*-Arylation of Isatin

This organic transformation was a three-step process. Initially, isatin was converted into its methyl isatin derivative, as summarized in Scheme 2. In the first step of the synthesis, deprotonation of isatin through alkylation was implemented by the treatment of isatin (**1**) with chloromethane in the presence of NaH (1.5 equivalent) in DMF for 6 h at 0 °C, which resulted in the formation of 1-methylisatin (**2**). In the subsequent step, generated **2** reacted with $\text{NH}_2\text{OH}\cdot\text{HCl}$ (1.2 equivalent) in ethanol to produce 1-methylisatin oxime (**3**) at 80 °C for 6 h.³⁷ To obtain the final product, isatin nitron derivatives **5a–g**, compound **3** was reacted with phenylboronic acid derivatives **4a–g** (1.2 equivalent) in a mixture of methanol and pyridine at 25 °C for 16 h, utilizing (0.1 equivalent) $\text{Cu}(\text{OAc})_2$ and (0.1 equivalent) CPIMCA as catalyst, as detailed in Scheme 2.³³

Result and Discussion

Characterizations

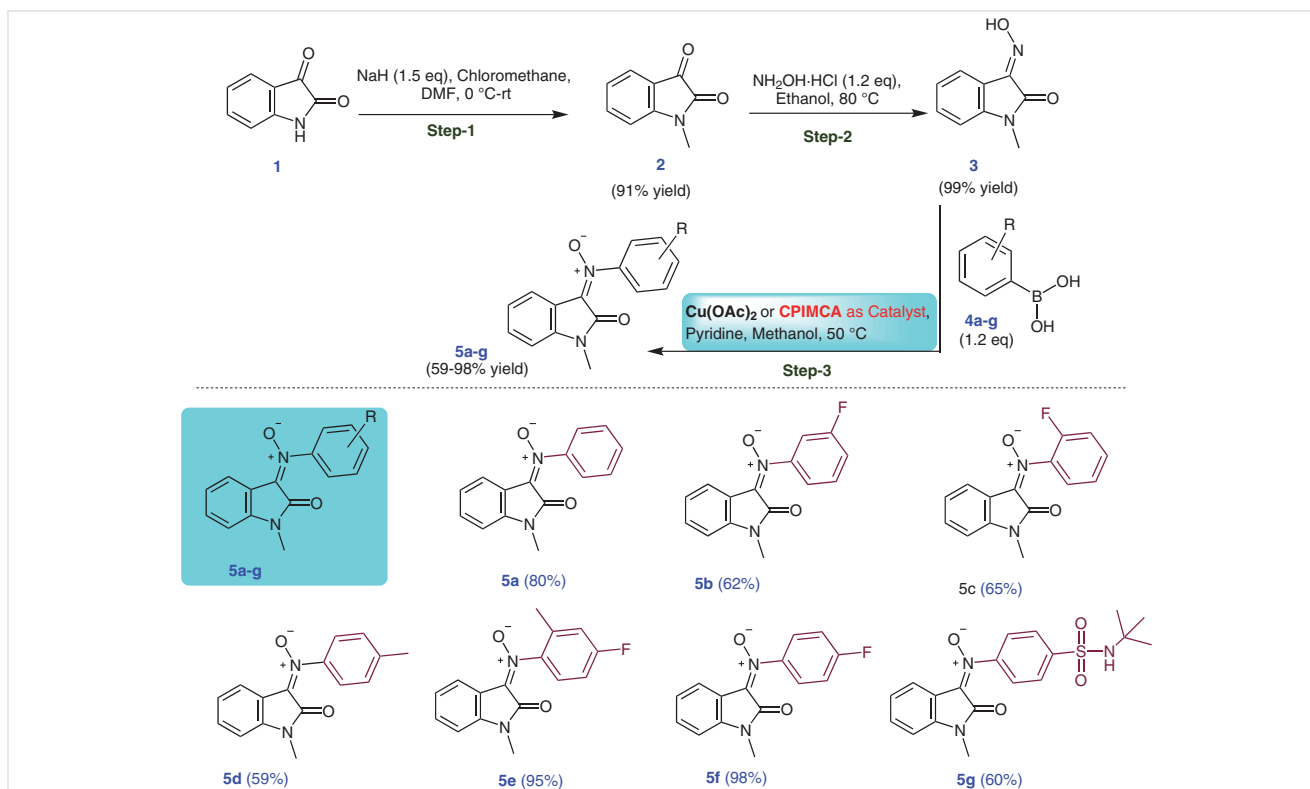
The functional group and chemical bonds of the CPIMCA were investigated by FTIR analysis in the range 4000–500 cm^{-1} . The results revealed peaks at 3443, 2920, 1623, 1265, and 1094 cm^{-1} in the spectra, as shown in Figure 1a. The detected peak at 3443 cm^{-1} corresponds to aliphatic amine (NH_2). The Peak at 2920 cm^{-1} represents the C–H component. Adsorption at 1623 cm^{-1} is attributed to C=C. The

peak at 1265 cm^{-1} corresponds to C–N from the aromatic amine, and the peak at 1094 cm^{-1} is attributed to C–C.^{38,39} It is noticeable that significant amounts of carbonaceous components C–C and C=C are present in the structure, and, after carbonization, some compounds such as hydroxyl and carboxyl groups will be eliminated either partially or completely.⁴⁰ Also, from comparison of the FTIR spectra of PDAI hydrogel and CPIM carbon aerogel, the presence of Cu and Fe is seen to influence the overall structure; we can see a shift in the peaks in the spectrum of aerogel⁴¹ that confirms the incorporation of Cu and Fe in the polymeric structure of CPIM carbon aerogel.

The magnetic properties of CPIMCA were analyzed by using VSM techniques. The sample was kept in the field range from –10000 to +10000 Oe at room temperature. From the hysteresis curve of the magnetization measurement of CPIMCA sample, it was observed that the sample is supermagnetic in nature and displayed an S-like curve, as depicted in Figure 1c. The saturation magnetization (M_s) value of the sample was 40.94 emu/g. Carbonization increased the magnetic saturation value and decreased the coercivity of the sample resulting in increased magnetization of the sample.^{42,43}

The magnetic behavior was also identified physically. On application of an external magnetic field, the sample was strongly attracted towards the magnet (Figure 1c), which is clearly useful for the catalytic applications of the magnetic sample.

XRD analysis was performed to determine the crystalline and amorphous nature of the sample. As demonstrated in Figure 1b, the peaks at $2\theta = 22.16^\circ$, 38.80° , and 43.70°



Scheme 2 Arylation of isatin oxime via catalytic coupling reaction with phenylboronic acid and comparative yield of nitron products

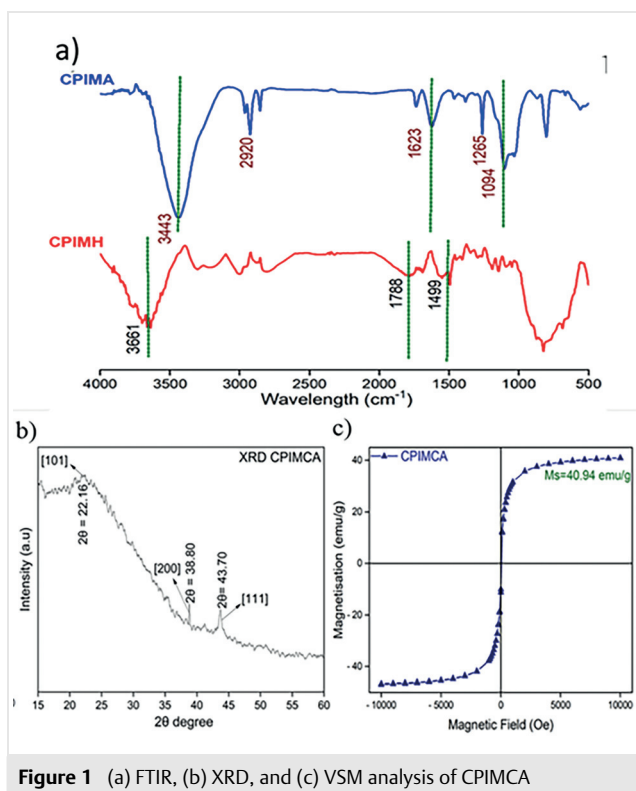


Figure 1 (a) FTIR, (b) XRD, and (c) VSM analysis of CPIMCA

correspond to the lattice planes [101], [200], and [111], respectively. The peak at 22.16° shows that the carbon skeleton of carbon aerogel is semi-crystalline in nature. The peak at 38.80° corresponds to Fe ions and the peak at 43.70° is consistent with Cu ions. From the XRD observations it can be concluded that copper and iron are completely encapsulated in the semi-crystalline Cu-doped magnetic carbon aerogel framework.^{44,45}

SEM, TEM, and EDX measurements were utilized to investigate the shape, morphology, particle size, elemental analysis, and particle length of the as-synthesized catalyst CPIMCA. As shown in Figure 2a and Figure 2b, SEM images at $10\ \mu\text{m}$ and $2\ \mu\text{m}$ demonstrated that the CPIMCA has an interconnected 3-D network structure, which reflects the proper binding of vinyl monomers via covalent interactions, which is further confirmed by TEM images. Alongside this, the material is clearly porous in nature and has the metal ions incorporated inside the carbon framework of the aerogel.^{46,47} It can also be confirmed that copper and iron particles are uniformly distributed throughout the polymeric structure. It is noticeable that after carbonization in an inert atmosphere, the 3-D polymeric structure remains porous. Furthermore, the elemental composition was confirmed by EDX-mapping, and the presence of Cu and Fe was also confirmed by the EDX image as depicted in Figure 2f. The SEM-EDX mapping images reveal that the carbon component covers the maximum area of the carbonized sample,

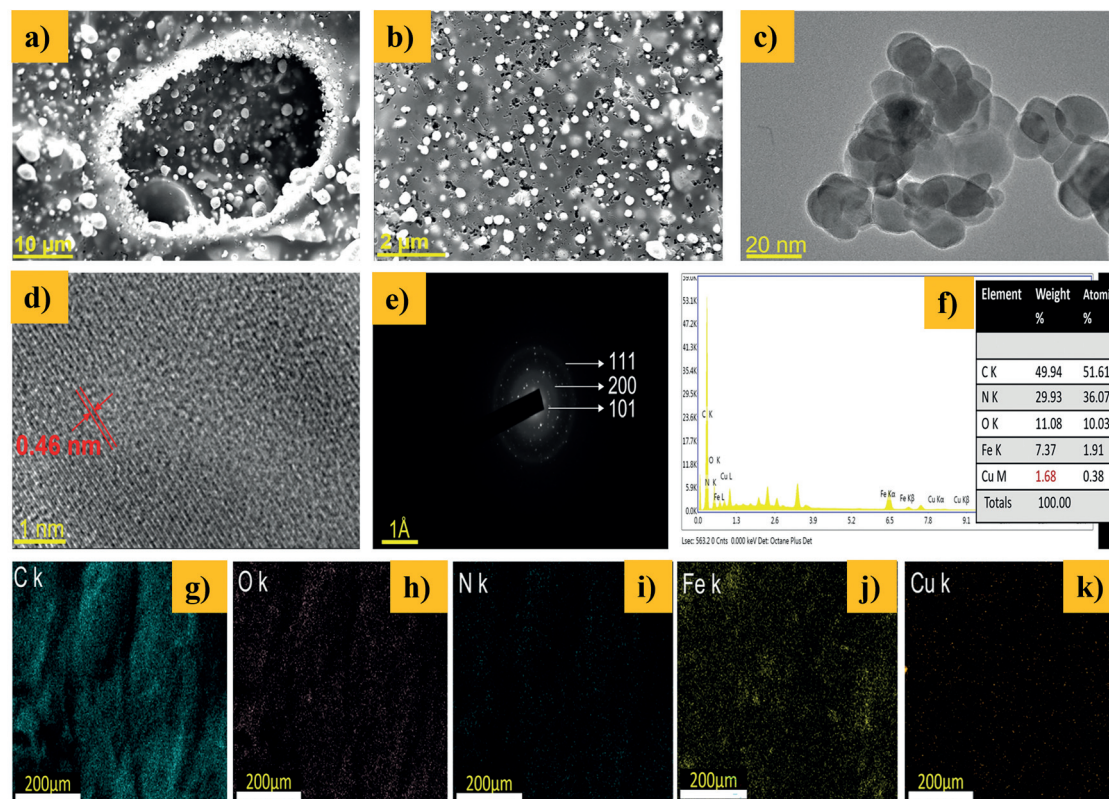


Figure 2 SEM (a) 10 μm (b) 2 μm ; TEM (c) 20 nm, (d) 1 nm; SAED 1 \AA (f) EDX image, elemental mapping images; (g) carbon, (h) oxygen, (i) nitrogen, (j) iron (k) copper of CPIMCa.

as shown in Figure 2g; along with this, copper and iron were embedded consistently in the structure, as exhibited in Figure 2j and Figure 2k, respectively. The analysis revealed that copper was present in 1.68% and Fe was present in the structure in 7.3%. The results also confirmed that carbon is present in the highest concentration; i.e., 49.94%, which indicates that the sample was carbonized as expected. Elements O and N were also spread homogeneously, as depicted in Figure 2h and Figure 2i, respectively. Interestingly, the encapsulation of the metals effectively increases the surface area and overall porosity of the material.

Moreover, the typical TEM images reveal more about the surface morphology of the CPIMCA, as can be seen in Figure 2c. At 20 nm in can be seen that the 3-D packed aerogel has Cu and Fe incorporated in a dense networked structure.^{48,49} It was observed that the mesoporous particles were formed with elliptical and spherical shapes with diameters of 12–30 nm. Additionally, the material exhibits lattice fringes in a single direction with a d-spacing of 0.46 nm, as illustrated in Figure 2d. In Figure 2e, the SAED pattern shows that the diffraction rings correspond to the [101], [200], and [111] lattice planes.

XPS analysis was used to predict the surface chemical composition and oxidation state of the elements present in the material. The XPS survey revealed five leading peaks: C 1s at 283 eV, N 1s at 400 eV, O 1s at 532 eV, Fe 2p at 724 eV, and Cu 2p at 974 eV, as shown in Figure 3a. The C 1s spectrum was deconvoluted into three peaks: first is a C-metal peak that appears at 284 eV, a peak at 284.63 that corresponds to (sp^2), and 285.55 eV is for C–C (sp^3), represented in Figure 3b. The N1s data, depicted in Figure 3d, shows the typical deconvoluted peaks at 397.89 eV and 400.18 eV correlating to N-metal and C–N, respectively. The data for O 1s, shown in Figure 3c, matched with the C=O at 531.2 eV, and O–C=O at 532.9 eV. The Cu 2p spectrum could fit three peaks and one satellite peak, which correspond to Cu 2p_{3/2} at 943 eV, Cu 2p_{1/2} at 950.6 eV, Cu O at 972.7 eV, and a satellite peak at 997 eV due to extra energy loss, as illustrated in Figure 3e. This data confirms that copper is present in two oxidation states.^{50,51} The Fe 2p data has been split into two peaks: 712.17 eV, which is assigned to Fe³⁺, and 725.23 eV, which belongs to Fe²⁺, supporting the observation that iron is present in two oxidation states as pictured in Figure 3f. Thus, upon carbonization, the copper is completely encapsulated inside the structure.^{52,53}

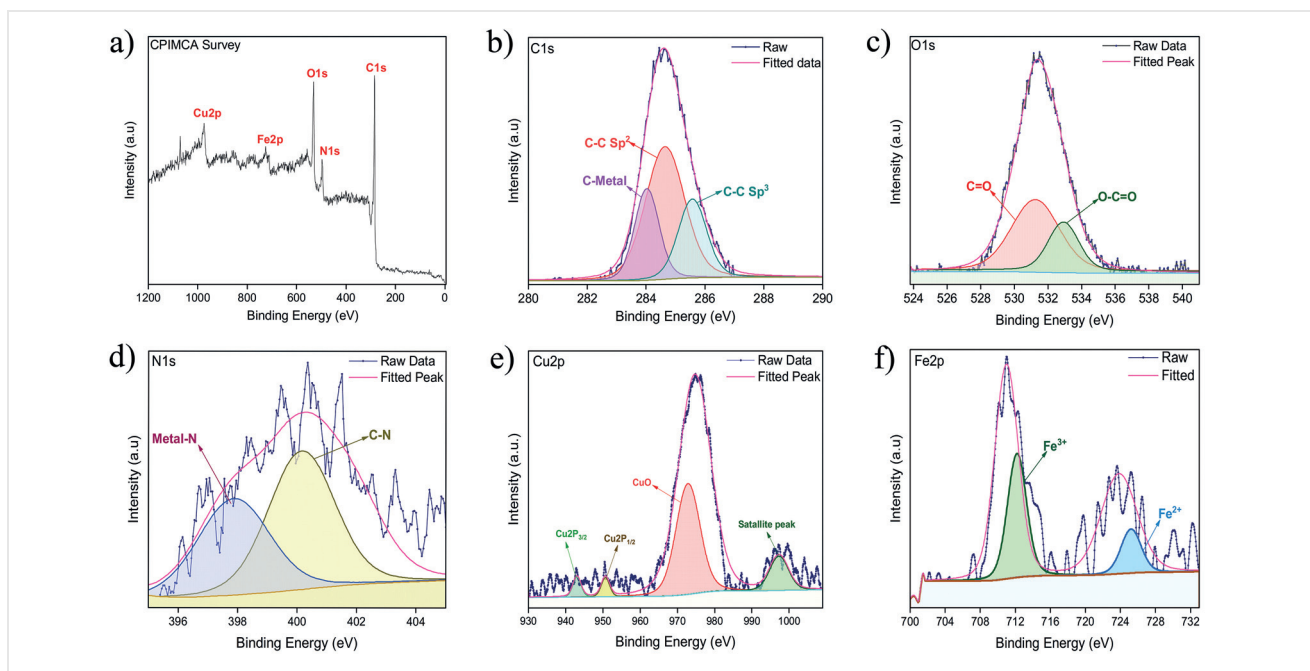


Figure 3 XPS of CPIMCA (a) Survey, (b) C 1s, (c) O 1s, (d) N 1s, (e) Cu 2p, (f) Fe 2p

Catalyst Investigation in Coupling Reaction

With the objective of examining the catalytic activity of the CPIMCA, the coupling reaction of isatin oxime with boronic acid derivatives was conducted to generate isatin nitrene derivatives (Figure 4). To our knowledge, this is the first time that metal doped magnetic carbon aerogel has been used as a catalyst for the formation of *N*-aryl nitrene products by *N*-arylation. In the preparation of isatin nitrene, initially isatin was converted into 1-methylisatin; thus, isatin, NaH, and chloromethane were used in a mole ratio of 1:2:1. Isatin was mixed in DMF, heterogeneous basic deprotonating agent NaH was added and the reaction mixture left for 6 h at 0 °C (the reaction was monitored by TLC and LC/MS). Upon completion, the mixture was diluted with EtOAc and washed with dilute HCl, to provide 1-methylisatin in 91% yield. To form the isatin oxime, a slurry of

1-methylisatin (31.77 mmol, 5.28 g) in ethanol (50 mL) was mixed with $\text{NH}_2\text{OH}\cdot\text{HCl}$ (47.66 mmol, 3.31 g) in H_2O (6 mL) and stirred at 80 °C for 6 h. The resulting greenish yellow paste was triturated with H_2O , filtered, washed with H_2O , and the subsequent product was dried overnight in a vacuum oven. In the final *N*-arylation step, 1-methylisatin oxime (1 equiv., 0.3 mmol) was mixed with phenyl boronic acid derivative (1.2 equiv.) and the reaction was started by the addition of catalyst CPIMCA (0.1 equiv, 0.002 equiv. Cu as 2% in CPIMCA catalyst) in the presence of anhydrous Na_2SO_4 , pyridine, and polar aprotic solvent methanol, and the reaction mixture was stirred for 16 h at 25 °C. Methanol was used because it is a renewable, green solvent. According to Byrne et al., methanol is a recommended renewable solvent, while solvents such as DCM, DCE, and toluene are either not safe or cannot be reused cost-effectively.⁵⁴

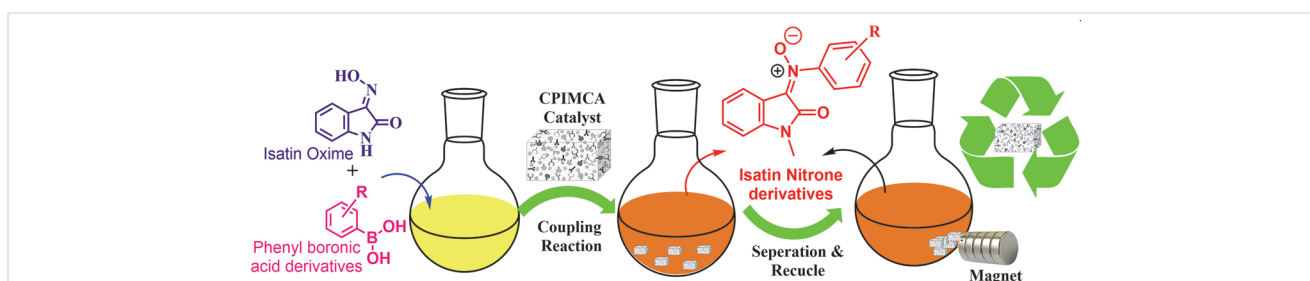
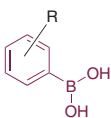
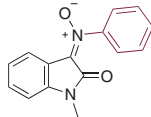
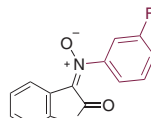
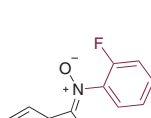
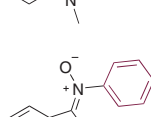
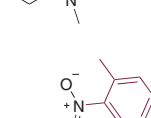
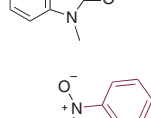
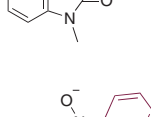


Figure 4 Assessing the catalytic activity of CPIMCA in the coupling reaction for the synthesis of isatin nitrene derivatives

Therefore, the use of a green solvent is a more environmentally compatible approach for this reaction procedure. The reaction was monitored by TLC and HRMS and the formation of the product was confirmed by ^1H NMR analysis. The compound was simply isolated by flash column chromatography. The catalytic investigation was conducted by comparing the catalytic activities of $\text{Cu}(\text{OAc})_2$ and CPIMCA.

The same set of reactions was done by using $\text{Cu}(\text{OAc})_2$ as catalyst (Scheme 2). Remarkably, the nitrono derivatives were obtained in up to 98% yield by using CPIMCA catalyst. As can be seen in Table 1 and Scheme 2, CPIMCA had significantly higher levels of catalytic activity than $\text{Cu}(\text{OAc})_2$. The yield of the products produced using the CPIMCA catalyst increased by 10–15%.

Table 1 Isatin Nitrono Derivatives Formed Using Different Catalysts

| Entry | Phenyl boronic acid 4 | Product isatin nitrono | Yield (%) | |
|-------|---|---|---------------------------|--------|
| | | | $\text{Cu}(\text{OAc})_2$ | CPIMCA |
| |  | | | |
| 1 | 4a R = H |  | 60 | 80 |
| 2 | 4b R = 3-F |  | 46 | 62 |
| 3 | 4c R = 2-F |  | 50 | 65 |
| 4 | 4d R = 4-Me |  | 40 | 59 |
| 5 | 4e R = 2-Me, 4-F |  | 80 | 95 |
| 6 | 4f R = 4-F |  | 82 | 98 |
| 7 | 4g R = 4-SO ₂ NH-tBu |  | 44 | 60 |

The CPIMCA catalyst showed good catalytic activity because the three-dimensional porous structure of the carbon aerogel provides a large surface area and an interconnected porous network, and the carbon framework allows uniform agglomeration in the structure leading more active catalytic sites. Moreover, incorporation of Cu and Fe ions in the carbon framework showed synergistic effects along with carbon, increasing its catalytic performance by facilitating the movement of electrons, which also allows better dispersion and accessibility of copper ions. Copper ions in $\text{Cu}(\text{OAc})_2$ are not as easily accessible, which can reduce the catalytic activity. Fe renders the aerogel magnetic, which enables easy separation from the reaction mixture by application of an external magnetic field. This makes the catalyst more sustainable and reduces waste.

Reusability of Catalyst

After the first cycle of compounds was completed, the CPIMCA catalyst was reused. The catalyst was recovered from the reaction mixture using an external magnet, then washed twice with ethanol and reused. The catalyst was used several times, and started losing its activity after three runs; the yield of the product reduced from 98 to 93% after three runs. However, no discernible shift was observed in the catalytic activity after repeated washing with ethanol; therefore, we may conclude that the activity of the catalyst was not lost overall.

Conclusion

In conclusion, the successful incorporation of copper and iron inside a magnetic PDAI carbon aerogel matrix provides a number of advantages for catalysis. Moreover, after carbonization (on heating at 800 °C) of the sample, the metals are doped inside the structure where they exhibit synergistic effects with the carbon polymeric matrix. The CPIMCA proved to be a competent catalyst with the synergistic effect of both the copper and iron facilitating the coupling reaction of isatin oxime and phenyl boronic acid derivatives. The products were formed in yields up to 98%, and the catalyst was easy to recover by using an external magnetic field as it did not agglomerate in the reaction mixture. The catalyst could be reused and gave similar results for three consecutive repetitions. Thus, CPIMCA can be used as competent catalyst for coupling reactions.

N-[3-(Dimethylamino)propyl]methacrylamide (DMAPMA), acrylic acid (AAc), *N*-vinyl imidazole (NVI), ammonium persulfate (APS), *N,N,N',N'*-tetramethyl ethylene diamine (TEMED), ferric(III) chloride ($\text{FeCl}_3 \cdot 6\text{H}_2\text{O}$), ferrous(II) sulfate ($\text{FeSO}_4 \cdot 7\text{H}_2\text{O}$), copper(II) chloride (CuCl_2), isatin, boronic acid derivatives, anhydrous Na_2SO_4 ,

pyridine, hydroxyl amine hydrochloride ($\text{NH}_2\text{OH} \cdot \text{HCl}$), nitrogen gas, sodium hydride (NaH), ethanol, methanol, dimethylformamide (DMF) and distilled water were used in the reaction.

The morphology of the synthesized CPIMCA was analyzed using X-ray diffraction spectroscopy with a Rigaku SmartlabSE X-ray diffractometer having voltage of 40 kV and a current of 30 mA, with a Cu-K α radiation in 2θ range 10–60°. For surface morphology, transition electron microscopy (TEM) images were captured with a JEOL JEM-2100F electron microscope supplied with a 200 kV accelerating voltage. The CPIMCA sample was drop-cast onto a copper-grid after dispersion and allowed to dry at room temperature. Scanning electron microscopy (SEM) and energy-dispersive X-ray (EDX) was performed with ZEISS, Merlin Compact, which has a tungsten electron and worked at a voltage of 20 kV, with Magnification $K \times 5$ to $K \times 10$. Prior to analysis the sample was coated with a thin layer of gold in a gold sputtering machine. For chemical morphology analysis, the sample was subject to Fourier transform infrared spectroscopy FTIR with a Perkin Elmer-Spectrum two FTIR analyser in the range 400–4000 cm^{-1} ; the sample was mixed with dry KBr prior to analysis as a KBr disk. To obtain magnetic measurements, vibrating sample magnetometry (VSM) was carried out with a Microsense-ADE-EV9 magnetometer with a magnetic field strength of up to 2.2 Tesla. The magnetic measurement range was –10000 to +10000 Oe. Furthermore, X-ray photoelectron spectroscopy (XPS; ULVAC-PHI, INC., PHI 5000 Versa Probe III Scanning XPS Microprobe) was utilized to determine the elemental composition, oxidation state, and binding energy. The NMR spectra of the products formed by the CPIMCA catalyzed reactions were recorded in $\text{DMSO}-d_6$ or MeOD with TMS as internal standard, with a Bruker 400 MHz instrument.

The NMR data of all the compounds are given in the Supporting Information.

1-Methyl-2-oxo-*N*-phenylindolin-3-imine Oxide (5a)

Yield: 35 mg (80%); brownish yellow liquid.

^1H NMR (400 MHz, $\text{DMSO}-d_6$): δ = 8.315–8.297 (d, J = 7.2 Hz, 1 H), 7.56–7.42 (m, 6 H), 7.155–7.098 (m, 2 H), 3.117 (s, 3 H).

^{13}C NMR (100 MHz, $\text{DMSO}-d_6$): δ = 25.91, 108.71, 117.6, 122.42, 123.82, 123.94, 128.77, 130.28, 132.29, 142.17, 146.405, 158.741.

HRMS (ESI): m/z [$M + H$] $^+$ calcd for $\text{C}_{15}\text{H}_{12}\text{N}_2\text{O}_2$: 253.0860; found: 253.0967.

N-(3-Fluorophenyl)-1-methyl-2-oxoindolin-3-imine Oxide (5b)

Yield: 37 mg (62%); orange-yellow solid.

^1H NMR (400 MHz, $\text{DMSO}-d_6$): δ = 8.30–8.281 (d, J = 7.6 Hz, 1 H), 7.675–7.438 (m, 3 H), 7.42–7.40 (m, 2 H), 7.162–1.109 (q, 2 H), 3.12 (s, 3 H).

^{13}C NMR (100 MHz, $\text{DMSO}-d_6$): δ = 25.95, 108.84, 117.13, 117.40, 122.51, 130.73, 132.57, 134.41, 142.38, 147.29, 158.74, 160.24, 162.68.

^{19}F NMR (400 MHz, $\text{DMSO}-d_6$): δ = –112.009.

HRMS (ESI): m/z [$M + H$] $^+$ calcd for $\text{C}_{15}\text{H}_{11}\text{FN}_2\text{O}_2$: 271.0801; found: 271.0874.

N-(2-Fluorophenyl)-1-methyl-2-oxoindolin-3-imine Oxide (5c)

Yield: 40 mg (65%); orange-yellow solid.

^1H NMR (400 MHz, $\text{DMSO}-d_6$): δ = 8.311–8.292 (d, J = 7.6 Hz, 1 H), 7.67–7.43 (m, 3 H), 7.361–7.400 (t, J = 8.0 Hz, 1 H), 7.13–7.16 (m, 2 H), 3.13 (s, 3 H).

^{13}C NMR (100 MHz, $\text{DMSO-}d_6$): $\delta = 25.95, 109.11, 116.26, 116.73, 122.72, 124.07, 125.24, 126.18, 132.17, 132.97, 134.12, 135.35, 142.37, 155.13, 158.42$.

^{19}F NMR (400 MHz, $\text{DMSO-}d_6$): $\delta = -125.989$.

HRMS (ESI): m/z [M + H] $^+$ calcd for $\text{C}_{15}\text{H}_{11}\text{FN}_2\text{O}_2$: 271.0801; found: 271.0877.

1-Methyl-2-oxo-N-(p-tolyl)indolin-3-imine Oxide (5d)

Yield: 25 mg (59%); orange-yellow solid.

^1H NMR (400 MHz, $\text{DMSO-}d_6$): $\delta = 8.304\text{--}8.286$ (d, $J = 7.2$ Hz, 1 H), 7.503–7.436 (m, 3 H), 7.313–7.293 (d, $J = 8.0$ Hz, 2 H), 7.145–7.090 (q, 2 H), 3.117 (s, 3 H), 2.98 (s, 3 H).

^{13}C NMR (100 MHz, $\text{DMSO-}d_6$): $\delta = 20.86, 25.927, 108.688, 117.748, 122.405, 123.755, 123.846, 129.098, 132.194, 133.897, 140.226, 142.071, 144.181, 158.769$.

HRMS (ESI): m/z [M + H] $^+$ calcd for $\text{C}_{16}\text{H}_{14}\text{N}_2\text{O}_2$: 267.1055; found: 267.1118.

N-(4-Fluoro-2-methylphenyl)-1-methyl-2-oxoindolin-3-imine Oxide (5e)

Yield: 50 mg (95%); orange-yellow solid.

^1H NMR (400 MHz, $\text{DMSO-}d_6$): $\delta = 8.320\text{--}8.303$ (d, $J = 6.8$ Hz, 1 H), 7.53–7.45 (m, 2 H), 7.30–7.27 (d, 1 H), 7.19–7.11 (m, 3 H), 3.11 (s, 3 H), 2.15 (s, 3 H).

^{13}C NMR (100 MHz, $\text{DMSO-}d_6$): $\delta = 16.09, 25.88, 108.84, 113.33, 116.97, 117.27, 122.50, 123.97, 126.23, 132.51, 134.13, 134.88, 142.36, 158.57, 160.67, 163.11$.

^{19}F NMR (400 MHz, $\text{DMSO-}d_6$): $\delta = -111.93$.

HRMS (ESI): m/z [M + H] $^+$ calcd for $\text{C}_{16}\text{H}_{13}\text{FN}_2\text{O}_2$: 285.0597; found: 285.1039.

N-(4-Fluorophenyl)-1-methyl-2-oxoindolin-3-imine Oxide (5f)

Yield: 52 mg (98%); orange-yellow solid.

^1H NMR (400 MHz, $\text{DMSO-}d_6$): $\delta = 8.285\text{--}8.30$ (d, $J = 7.2$ Hz, 1 H), 7.688–7.653 (m, 2 H), 7.51–7.47 (t, 1 H), 7.334–7.379 (t, $J = 8.0$ Hz, 2 H), 7.15–7.103 (m, 2 H), 3.121 (s, 3 H).

^{13}C NMR (100 MHz, $\text{DMSO-}d_6$): $\delta = 25.90, 108.70, 115.53, 115.76, 117.55, 122.42, 123.85, 126.58, 132.34, 134.25, 142.17, 142.68, 158.79, 161.34, 163.79$.

^{19}F NMR (400 MHz, $\text{DMSO-}d_6$): $\delta = -110.35$.

HRMS (ESI): m/z [M + H] $^+$ calcd for $\text{C}_{15}\text{H}_{11}\text{FN}_2\text{O}_2$: 271.0801; found: 271.0869.

N-(4-(N-(tert-Butyl)sulfamoyl)phenyl)-1-methyl-2-oxoindolin-3-imine Oxide (5g)

Yield: 36 mg (60%); orange-yellow solid.

^1H NMR (400 MHz, $\text{DMSO-}d_6$): $\delta = 8.287\text{--}8.307$ (d, $J = 8.0$, 1 H), 7.937–7.958 (d, $J = 8.4$, 2 H), 7.770–7.783 (d, $J = 5.2$ Hz, 2 H), 7.496–7.534 (t, $J = 8.0$ Hz, 1 H), 7.172–7.120 (m, 2 H), 3.13 (s, 3 H), 1.13 (s, 9 H).

^{13}C NMR (100 MHz, $\text{DMSO-}d_6$): $\delta = 26.001, 29.793, 53.541, 108.91, 117.35, 122.57, 124.055, 124.948, 127.09, 132.696, 134.665, 142.476, 145.712, 148.166, 158.782$.

HRMS (ESI): m/z [M + H] $^+$ calcd for $\text{C}_{19}\text{H}_{21}\text{N}_3\text{O}_4\text{S}$: 388.2176; found: 388.1319.

Conflict of Interest

The authors declare no conflict of interest.

Funding Information

The authors thank the Science and Engineering Research Board, New Delhi for financial support through the SERB-TARE Project (TAR/2022/000673).

Acknowledgment

Authors acknowledge the Amity Institute of Click Chemistry Research and Studies (AICCRS), Amity University, Noida; the University of Delhi and Dr. Vinod Kumar (Assistant Professor, Jawaharlal Nehru University, New Delhi) for providing the instrumentation facilities. The authors are also thankful to Dr. Gaurav Srivastava (Aragen Life Sciences Private Limited, Hyderabad) for the innovative Industry-Academia Collaboration with Amity University for advancing research and knowledge, for creating a skilled workforce, and for his guidance as an external co-guide of DM.

Supporting Information

Supporting information for this article is available online at <https://doi.org/10.1055/a-2182-7757>.

References

- (1) Farzaliyev, V.; Shuriberko, A.; Sujayey, A.; Osmanova, S.; Gojayeva, S.; Gahramanova, K. *J. Mol. Struct.* **2020**, *1221*, 128844.
- (2) Kaushal, A.; Bhukya, J.; Yadav, A. K.; Mishra, V.; Kumar, D. *Tetrahedron Lett.* **2023**, 154742.
- (3) Kumar, V.; Saha, R.; Chatterjee, S.; Mishra, V. *React. Chem. Eng.* **2023**, *8*, 2677.
- (4) Son, G. M.; Truong, C. C.; Mishra, D. K.; Mishra, V.; Kim, Y. J. *Bull. Korean Chem. Soc.* **2018**, *39*, 174.
- (5) Yen, C.-T.; Liu, Y.-H.; Peng, S.-M.; Liu, S.-T. *Org. Lett.* **2022**, *24*, 3373.
- (6) Dai, S.; Chou, J. P.; Wang, K. W.; Hsu, Y. Y.; Hu, A.; Pan, X.; Chen, T. Y. *Nat. Commun.* **2019**, *10*, 440.
- (7) Yang, Y.; Reber, A. C.; Gilliland, S. E. III.; Castano, C. E.; Gupton, B. F.; Khanna, S. N. *J. Catal.* **2018**, *360*, 20.
- (8) Fernández, E.; Rivero-Crespo, M. A.; Dominguez, I.; Rubio-Marques, P.; Oliver-Meseguer, J.; Liu, L.; Cabereo-Antonino, M.; Gavara, R.; Hernandez-Garrido, J. C.; Boronat, M.; Levya-Perez, A. *J. Am. Chem. Soc.* **2019**, *141*, 1928.
- (9) Baran, T. J. *Colloid Interface Sci.* **2017**, *496*, 446.
- (10) Zhang, Z.; Zhao, Z.; Hou, Y.; Wang, H.; Li, X.; He, G.; Zhang, M. *Angew. Chem. Int. Ed.* **2019**, *58*, 8862.
- (11) Oh, S. G.; Mishra, V.; Cho, J. K.; Kim, B. J.; Kim, H. S.; Suh, Y. W.; Lee, H.; Park, H. S.; Kim, Y. J. *Catal. Commun.* **2014**, *43*, 79.
- (12) Ming, X.-X.; Wu, S.; Tian, Z.-Y.; Song, J.-W.; Zhang, C.-P. *Org. Lett.* **2021**, *23*, 6795.
- (13) Devendar, P.; Qu, R. Y.; Kang, W. M.; He, B.; Yang, G. F. *J. Agric. Food Chem.* **2018**, *66*, 8914.
- (14) Karbowska, B. *Environ. Monit. Assess.* **2016**, 188.

- (15) Truong, C. C.; Mishra, D. K.; Mishra, V. *Organic carbonate as a green solvent for biocatalysis*, In *Green Sustainable Process for Chemical and Environmental Engineering and Science*; Elsevier: Amsterdam, Netherlands, **2021**, 253–275.
- (16) Panda, S. K.; Aggarwal, I.; Kumar, H.; Prasad, L.; Kumar, A.; Sharma, A.; Vo, D. V. N.; Van Thuan, D.; Mishra, V. *Environ. Chem. Lett.* **2021**, *19*, 2487.
- (17) Jindal, S.; Anand, R.; Sharma, N.; Yadav, N.; Mudgal, D.; Mishra, R.; Mishra, V. *ACS Appl. Electron. Mater.* **2022**, *4*, 2146.
- (18) Yadav, N.; Gaikwad, R. P.; Mishra, V.; Gawande, M. B. *Bull. Chem. Soc. Jpn.* **2022**, *95*, 1638.
- (19) Mishra, V.; Cho, J. K.; Shin, S. H.; Suh, Y. W.; Kim, H. S.; Kim, Y. J. *Appl. Catal., A* **2014**, *487*, 82.
- (20) Kumar, M.; Verma, S.; Mishra, V.; Reiser, O.; Verma, A. K. *J. Org. Chem.* **2022**, *87*, 6263.
- (21) Veerakumar, P.; Thanasekaran, P.; Subburaj, T.; Lin, K.-C. *C* **2018**, *4*, 54.
- (22) Karoyo, A. H.; Wilson, L. D. *Materials* **2021**, *14*, 1095.
- (23) Pekel, N.; Güven, O. *Polym. Bull.* **2004**, *51*, 307.
- (24) Mishra, V.; Kumar, R. *Carbohydr. Polym.* **2011**, *83*, 1534.
- (25) Mishra, V.; Jung, S. H.; Park, J. M.; Jeong, H. M.; Lee, H. I. *Macromol. Rapid Commun.* **2014**, *35*, 442.
- (26) Mishra, V.; Kumar, R. *J. Appl. Polym. Sci.* **2013**, *128*, 3295.
- (27) Bhunia, S.; Pawar, G. G.; Kumar, S. V.; Jiang, Y.; Ma, D. *Angew. Chem. Int. Ed.* **2017**, *56*, 16136.
- (28) Sharma, S.; Kaur, M.; Sharma, C.; Choudhary, A.; Paul, S. *ACS Omega* **2021**, *6*, 19529.
- (29) Panda, N.; Jena, A. K. *Org. Chem.: Curr. Res.* **2015**, *4*, 1000130.
- (30) Shirakawa, E.; Ikeda, D.; Masui, S.; Yoshida, M.; Hayashi, T. *J. Am. Chem. Soc.* **2012**, *134*, 272.
- (31) Liu, L.; Corma, A. *Chem. Rev.* **2018**, *118*, 4981.
- (32) Mo, X. L.; Chen, C. H.; Liang, C.; Mo, D. L. *Eur. J. Org. Chem.* **2018**, *150*.
- (33) Chen, C. H.; Liu, Q. Q.; Ma, X. P.; Feng, Y.; Liang, C.; Pan, C. X.; Su, G. F.; Mo, D. L. *J. Org. Chem.* **2017**, *82*, 6417.
- (34) Arkaban, H.; Barani, M.; Akbarizadeh, M. R.; Chauhan, N. P. S.; Jadoun, S.; Soltani, M. D.; Zarrintaj, P. *Polymers* **2022**, *14*, 1259.
- (35) Li, Y.; Huang, G.; Zhang, X.; Li, B.; Chen, Y.; Lu, T.; Lu, T. J.; Xu, F. *Adv. Funct. Mater.* **2013**, *23*, 660.
- (36) He, X.; Zhang, L.; Meng, D.; Wu, J. *Eur. Polym. J.* **2017**, *89*, 461.
- (37) Saczewski, J.; Paluchowska, A.; Klenc, J.; Raux, E.; Barnes, S.; Sullivan, S.; Duszynska, B.; Bojarski, A. J.; Strekowski, L. *J. Heterocycl. Chem.* **2009**, *46*, 1259.
- (38) Yang, Z.; Peng, H.; Wang, W.; Liu, T. *J. Appl. Polym. Sci.* **2010**, *116*, 2658.
- (39) Esfahani, M. Z.; Aghaei, A.; Khosravi, M.; Bagheri, N.; Khakpour, Z.; Javaheri, M. *New J. Chem.* **2017**, *41*, 11731.
- (40) Mohsenpour, M.; Motahari, S.; Tajabadi, F.; Najafi, M. *RSC Adv.* **2020**, *10*, 41780.
- (41) Slimi, O.; Djouadi, D.; Hammiche, L.; Chelouche, A.; Touam, T. *J. Porous Mater.* **2018**, *25*, 595.
- (42) Ye, S.; Jin, W.; Huang, Q.; Hu, Y.; Li, Y.; Li, B. *Int. J. Biol. Macromol.* **2016**, *92*, 1169.
- (43) Andrew, L. J.; Gillman, E. R.; Walters, C. M.; Lizundia, E.; MacLachlan, M. J. *Small* **2023**, 2301947.
- (44) Zhai, Z.; Ren, B.; Xu, Y.; Wang, S.; Zhang, L.; Liu, Z. *IOP Conf. Ser. Earth Environ. Sci.* **2020**, 508.
- (45) Kreek, K.; Kulp, M.; Uibu, M.; Mere, A.; Koel, M. *Oil Shale* **2014**, *31*, 185.
- (46) Pang, Y.; Mo, Z.; Wang, H.; Linkov, V.; Wang, X.; Wang, R. *Catal. Sci. Technol.* **2020**, *10*, 5288.
- (47) Yang, M.; Wang, H.; Jin, S.; Zhang, R.; Wang, Y.; Huo, W.; Wang, X.; Jin, M.; Qiao, W.; Ling, L. *Catal. Sci. Technol.* **2021**, *11*, 2057.
- (48) Ahamad, T.; Naushad, M.; Ruksana, ; Alhabarah, A. N.; Alshehri, S. M. *Int. J. Biol. Macromol.* **2019**, *132*, 1031.
- (49) Reyhani, R.; Zadhoush, A.; Tabrizi, N. S.; Nazockdast, H.; Naeimirad, M. *J. Non-Cryst. Solids* **2021**, *571*, 7073.
- (50) Zhai, Z.; Ren, B.; Xu, Y.; Wang, S.; Zhang, L.; Liu, Z. *Org. Electron.* **2019**, *70*, 246.
- (51) Fu, R.; Yoshizawa, N.; Dresselhaus, M. S.; Dresselhaus, G.; Satcher, J. H.; Baumann, T. F. *Langmuir* **2002**, *18*, 10100.
- (52) Wang, S.; Xu, Y.; Yan, M.; Zhai, Z.; Ren, B.; Zhang, L.; Liu, Z. *J. Electroanal. Chem.* **2018**, *809*, 111.
- (53) Dong, X.; Xu, Y.; Wang, S.; Zhao, J.; Ren, B.; Zhang, L.; Liu, Z. *Materials* **2018**, *11*.
- (54) Byrne, F. P.; Jin, S.; Paggiola, G.; Petchey, T. H.; Clark, J. H.; Farmer, T. J.; Hunt, A. J.; McElroy, C. R.; Sherwood, J. *Sustainable Chem. Processes.* **2016**, *4*.